

# Measurement of Event Shape Variables in Deep Inelastic $e p$ Scattering

H1 Collaboration

## Abstract

Deep inelastic  $e p$  scattering data, taken with the H1 detector at HERA, are used to study the event shape variables thrust, jet broadening and jet mass in the current hemisphere of the Breit frame over a large range of momentum transfers  $Q$  between 7 GeV and 100 GeV. The data are compared with results from  $e^+e^-$  experiments. Using second order QCD calculations and an approach to relate hadronisation effects to power corrections an analysis of the  $Q$  dependences of the means of the event shape parameters is presented, from which both the power corrections and the strong coupling constant are determined without any assumption on fragmentation models. The power corrections of all event shape variables investigated follow a  $1/Q$  behaviour and can be described by a common parameter  $\bar{\alpha}_0$ .

*Submitted to Physics Letters B*

C. Adloff<sup>35</sup>, S. Aid<sup>13</sup>, M. Anderson<sup>23</sup>, V. Andreev<sup>26</sup>, B. Andrieu<sup>29</sup>, V. Arkadov<sup>36</sup>, C. Arndt<sup>11</sup>,  
 I. Ayyaz<sup>30</sup>, A. Babaev<sup>25</sup>, J. Bähr<sup>36</sup>, J. Bán<sup>18</sup>, P. Baranov<sup>26</sup>, E. Barrelet<sup>30</sup>, R. Barschke<sup>11</sup>,  
 W. Bartel<sup>11</sup>, U. Bassler<sup>30</sup>, H.P. Beck<sup>38</sup>, M. Beck<sup>14</sup>, H.-J. Behrend<sup>11</sup>, A. Belousov<sup>26</sup>,  
 Ch. Berger<sup>1</sup>, G. Bernardi<sup>30</sup>, G. Bertrand-Coremans<sup>4</sup>, R. Beyer<sup>11</sup>, P. Biddulph<sup>23</sup>, J.C. Bizot<sup>28</sup>,  
 K. Borrás<sup>8</sup>, F. Botterweck<sup>27</sup>, V. Boudry<sup>29</sup>, S. Bourov<sup>25</sup>, A. Braemer<sup>15</sup>, W. Braunschweig<sup>1</sup>,  
 V. Brisson<sup>28</sup>, D.P. Brown<sup>23</sup>, W. Brückner<sup>14</sup>, P. Bruel<sup>29</sup>, D. Bruncko<sup>18</sup>, C. Brune<sup>16</sup>, J. Bürger<sup>11</sup>,  
 F.W. Büsler<sup>13</sup>, A. Buniatian<sup>4</sup>, S. Burke<sup>19</sup>, G. Buschhorn<sup>27</sup>, D. Calvet<sup>24</sup>, A.J. Campbell<sup>11</sup>,  
 T. Carli<sup>27</sup>, M. Charlet<sup>11</sup>, D. Clarke<sup>5</sup>, B. Clerbaux<sup>4</sup>, S. Cocks<sup>20</sup>, J.G. Contreras<sup>8</sup>,  
 C. Cormack<sup>20</sup>, J.A. Coughlan<sup>5</sup>, M.-C. Cousinou<sup>24</sup>, B.E. Cox<sup>23</sup>, G. Cozzika<sup>9</sup>, D.G. Cussans<sup>5</sup>,  
 J. Cvach<sup>31</sup>, S. Dagoret<sup>30</sup>, J.B. Dainton<sup>20</sup>, W.D. Dau<sup>17</sup>, K. Daum<sup>40</sup>, M. David<sup>9</sup>, A. De Roeck<sup>11</sup>,  
 E.A. De Wolf<sup>4</sup>, B. Delcourt<sup>28</sup>, M. Dirkmann<sup>8</sup>, P. Dixon<sup>19</sup>, W. Dlugosz<sup>7</sup>, C. Dollfus<sup>38</sup>,  
 K.T. Donovan<sup>21</sup>, J.D. Dowell<sup>3</sup>, H.B. Dreis<sup>2</sup>, A. Droutskoi<sup>25</sup>, J. Ebert<sup>35</sup>, T.R. Ebert<sup>20</sup>,  
 G. Eckerlin<sup>11</sup>, V. Efremenko<sup>25</sup>, S. Egli<sup>38</sup>, R. Eichler<sup>37</sup>, F. Eisele<sup>15</sup>, E. Eisenhandler<sup>21</sup>,  
 E. Elsen<sup>11</sup>, M. Erdmann<sup>15</sup>, A.B. Fahr<sup>13</sup>, L. Favart<sup>28</sup>, A. Fedotov<sup>25</sup>, R. Felst<sup>11</sup>, J. Feltesse<sup>9</sup>,  
 J. Ferencei<sup>18</sup>, F. Ferrarotto<sup>33</sup>, K. Flamm<sup>11</sup>, M. Fleischer<sup>8</sup>, M. Flieser<sup>27</sup>, G. Flügge<sup>2</sup>,  
 A. Fomenko<sup>26</sup>, J. Formánek<sup>32</sup>, J.M. Foster<sup>23</sup>, G. Franke<sup>11</sup>, E. Gabathuler<sup>20</sup>, K. Gabathuler<sup>34</sup>,  
 F. Gaede<sup>27</sup>, J. Garvey<sup>3</sup>, J. Gayler<sup>11</sup>, M. Gebauer<sup>36</sup>, R. Gerhards<sup>11</sup>, A. Glazov<sup>36</sup>, L. Goerlich<sup>6</sup>,  
 N. Gogitidze<sup>26</sup>, M. Goldberg<sup>30</sup>, B. Gonzalez-Pineiro<sup>30</sup>, I. Gorelov<sup>25</sup>, C. Grab<sup>37</sup>, H. Grässler<sup>2</sup>,  
 T. Greenshaw<sup>20</sup>, R.K. Griffiths<sup>21</sup>, G. Grindhammer<sup>27</sup>, A. Gruber<sup>27</sup>, C. Gruber<sup>17</sup>, T. Hadig<sup>1</sup>,  
 D. Haidt<sup>11</sup>, L. Hajduk<sup>6</sup>, T. Haller<sup>14</sup>, M. Hampel<sup>1</sup>, W.J. Haynes<sup>5</sup>, B. Heinemann<sup>11</sup>,  
 G. Heinzelmann<sup>13</sup>, R.C.W. Henderson<sup>19</sup>, S. Hengstmann<sup>38</sup>, H. Henschel<sup>36</sup>, I. Herynek<sup>31</sup>,  
 M.F. Hess<sup>27</sup>, K. Hewitt<sup>3</sup>, K.H. Hiller<sup>36</sup>, C.D. Hilton<sup>23</sup>, J. Hladký<sup>31</sup>, M. Höppner<sup>8</sup>,  
 D. Hoffmann<sup>11</sup>, T. Holtom<sup>20</sup>, R. Horisberger<sup>34</sup>, V.L. Hudgson<sup>3</sup>, M. Hütte<sup>8</sup>, M. Ibbotson<sup>23</sup>,  
 Ç. İssever<sup>8</sup>, H. Itterbeck<sup>1</sup>, M. Jacquet<sup>28</sup>, M. Jaffre<sup>28</sup>, J. Janoth<sup>16</sup>, D.M. Jansen<sup>14</sup>, L. Jönsson<sup>22</sup>,  
 D.P. Johnson<sup>4</sup>, H. Jung<sup>22</sup>, P.I.P. Kalmus<sup>21</sup>, M. Kander<sup>11</sup>, D. Kant<sup>21</sup>, U. Kathage<sup>17</sup>,  
 J. Katzy<sup>15</sup>, H.H. Kaufmann<sup>36</sup>, O. Kaufmann<sup>15</sup>, M. Kausch<sup>11</sup>, S. Kazarian<sup>11</sup>, I.R. Kenyon<sup>3</sup>,  
 S. Kermiche<sup>24</sup>, C. Keuker<sup>1</sup>, C. Kiesling<sup>27</sup>, M. Klein<sup>36</sup>, C. Kleinwort<sup>11</sup>, G. Knies<sup>11</sup>, T. Köhler<sup>1</sup>,  
 J.H. Köhne<sup>27</sup>, H. Kolanoski<sup>39</sup>, S.D. Kolya<sup>23</sup>, V. Korbel<sup>11</sup>, P. Kostka<sup>36</sup>, S.K. Kotelnikov<sup>26</sup>,  
 T. Krämerkämper<sup>8</sup>, M.W. Krasny<sup>6,30</sup>, H. Krehbiel<sup>11</sup>, D. Krücker<sup>27</sup>, A. Küpper<sup>35</sup>, H. Küster<sup>22</sup>,  
 M. Kuhlen<sup>27</sup>, T. Kurča<sup>36</sup>, B. Laforge<sup>9</sup>, M.P.J. Landon<sup>21</sup>, W. Lange<sup>36</sup>, U. Langenegger<sup>37</sup>,  
 A. Lebedev<sup>26</sup>, F. Lehner<sup>11</sup>, V. Lemaitre<sup>11</sup>, S. Levonian<sup>29</sup>, M. Lindstroem<sup>22</sup>, F. Linsel<sup>11</sup>,  
 J. Lipinski<sup>11</sup>, B. List<sup>11</sup>, G. Lobo<sup>28</sup>, G.C. Lopez<sup>12</sup>, V. Lubimov<sup>25</sup>, D. Lüke<sup>8,11</sup>, L. Lytkin<sup>14</sup>,  
 N. Magnussen<sup>35</sup>, H. Mahlke-Krüger<sup>11</sup>, E. Malinowski<sup>26</sup>, R. Maraček<sup>18</sup>, P. Marage<sup>4</sup>, J. Marks<sup>15</sup>,  
 R. Marshall<sup>23</sup>, J. Martens<sup>35</sup>, G. Martin<sup>13</sup>, R. Martin<sup>20</sup>, H.-U. Martyn<sup>1</sup>, J. Martyniak<sup>6</sup>,  
 T. Mavroidis<sup>21</sup>, S.J. Maxfield<sup>20</sup>, S.J. McMahon<sup>20</sup>, A. Mehta<sup>5</sup>, K. Meier<sup>16</sup>, P. Merkel<sup>11</sup>,  
 F. Metlica<sup>14</sup>, A. Meyer<sup>13</sup>, A. Meyer<sup>11</sup>, H. Meyer<sup>35</sup>, J. Meyer<sup>11</sup>, P.-O. Meyer<sup>2</sup>, A. Migliori<sup>29</sup>,  
 S. Mikocki<sup>6</sup>, D. Milstead<sup>20</sup>, J. Moeck<sup>27</sup>, F. Moreau<sup>29</sup>, J.V. Morris<sup>5</sup>, E. Mroczko<sup>6</sup>, D. Müller<sup>38</sup>,  
 K. Müller<sup>11</sup>, P. Murín<sup>18</sup>, V. Nagovizin<sup>25</sup>, R. Nahnhauser<sup>36</sup>, B. Naroska<sup>13</sup>, Th. Naumann<sup>36</sup>,  
 I. Négri<sup>24</sup>, P.R. Newman<sup>3</sup>, D. Newton<sup>19</sup>, H.K. Nguyen<sup>30</sup>, T.C. Nicholls<sup>3</sup>, F. Niebergall<sup>13</sup>,  
 C. Niebuhr<sup>11</sup>, Ch. Niedzballa<sup>1</sup>, H. Niggli<sup>37</sup>, G. Nowak<sup>6</sup>, T. Nunnemann<sup>14</sup>, H. Oberlack<sup>27</sup>,  
 J.E. Olsson<sup>11</sup>, D. Ozerov<sup>25</sup>, P. Palmen<sup>2</sup>, E. Panaro<sup>11</sup>, A. Panitch<sup>4</sup>, C. Pascaud<sup>28</sup>,  
 S. Passaggio<sup>37</sup>, G.D. Patel<sup>20</sup>, H. Pawletta<sup>2</sup>, E. Peppel<sup>36</sup>, E. Perez<sup>9</sup>, J.P. Phillips<sup>20</sup>,  
 A. Pieuchot<sup>24</sup>, D. Pitzl<sup>37</sup>, R. Pöschl<sup>8</sup>, G. Pope<sup>7</sup>, B. Povh<sup>14</sup>, K. Rabbertz<sup>1</sup>, P. Reimer<sup>31</sup>,  
 H. Rick<sup>8</sup>, S. Riess<sup>13</sup>, E. Rizvi<sup>21</sup>, P. Robmann<sup>38</sup>, R. Roosen<sup>4</sup>, K. Rosenbauer<sup>1</sup>, A. Rostovtsev<sup>30</sup>,  
 F. Rouse<sup>7</sup>, C. Royon<sup>9</sup>, K. Rüter<sup>27</sup>, S. Rusakov<sup>26</sup>, K. Rybicki<sup>6</sup>, D.P.C. Sankey<sup>5</sup>, P. Schacht<sup>27</sup>,  
 S. Schiek<sup>11</sup>, S. Schleich<sup>16</sup>, P. Schleper<sup>15</sup>, W. von Schlippe<sup>21</sup>, D. Schmidt<sup>35</sup>, G. Schmidt<sup>11</sup>,  
 L. Schoeffel<sup>9</sup>, A. Schöning<sup>11</sup>, V. Schröder<sup>11</sup>, E. Schuhmann<sup>27</sup>, B. Schwab<sup>15</sup>, F. Sefkow<sup>38</sup>,

A. Semenov<sup>25</sup>, V. Shekelyan<sup>11</sup>, I. Sheviakov<sup>26</sup>, L.N. Shtarkov<sup>26</sup>, G. Siegmon<sup>17</sup>, U. Siewert<sup>17</sup>, Y. Sirois<sup>29</sup>, I.O. Skillicorn<sup>10</sup>, T. Sloan<sup>19</sup>, P. Smirnov<sup>26</sup>, M. Smith<sup>20</sup>, V. Solochenko<sup>25</sup>, Y. Soloviev<sup>26</sup>, A. Specka<sup>29</sup>, J. Spiekermann<sup>8</sup>, S. Spielman<sup>29</sup>, H. Spitzer<sup>13</sup>, F. Squinabol<sup>28</sup>, P. Steffen<sup>11</sup>, R. Steinberg<sup>2</sup>, J. Steinhart<sup>13</sup>, B. Stella<sup>33</sup>, A. Stellberger<sup>16</sup>, J. Stiewe<sup>16</sup>, U. Stöblein<sup>36</sup>, K. Stolze<sup>36</sup>, U. Straumann<sup>15</sup>, W. Struczinski<sup>2</sup>, J.P. Sutton<sup>3</sup>, S. Tapprogge<sup>16</sup>, M. Taševský<sup>32</sup>, V. Tchernyshov<sup>25</sup>, S. Tchetchelnitski<sup>25</sup>, J. Theissen<sup>2</sup>, G. Thompson<sup>21</sup>, P.D. Thompson<sup>3</sup>, N. Tobien<sup>11</sup>, R. Todenhagen<sup>14</sup>, P. Truöl<sup>38</sup>, G. Tsipolitis<sup>37</sup>, J. Turnau<sup>6</sup>, E. Tzamariudaki<sup>11</sup>, P. Uelkes<sup>2</sup>, A. Usik<sup>26</sup>, S. Valkár<sup>32</sup>, A. Valkárová<sup>32</sup>, C. Vallée<sup>24</sup>, P. Van Esch<sup>4</sup>, P. Van Mechelen<sup>4</sup>, D. Vandenplas<sup>29</sup>, Y. Vazdik<sup>26</sup>, P. Verrecchia<sup>9</sup>, G. Villet<sup>9</sup>, K. Wacker<sup>8</sup>, A. Wagener<sup>2</sup>, M. Wagener<sup>34</sup>, R. Wallny<sup>15</sup>, T. Walter<sup>38</sup>, B. Waugh<sup>23</sup>, G. Weber<sup>13</sup>, M. Weber<sup>16</sup>, D. Wegener<sup>8</sup>, A. Wegner<sup>27</sup>, T. Wengler<sup>15</sup>, M. Werner<sup>15</sup>, L.R. West<sup>3</sup>, S. Wiesand<sup>35</sup>, T. Wilksen<sup>11</sup>, S. Willard<sup>7</sup>, M. Winde<sup>36</sup>, G.-G. Winter<sup>11</sup>, C. Wittek<sup>13</sup>, M. Wobisch<sup>2</sup>, H. Wollatz<sup>11</sup>, E. Wünsch<sup>11</sup>, J. Žáček<sup>32</sup>, D. Zarbock<sup>12</sup>, Z. Zhang<sup>28</sup>, A. Zhokin<sup>25</sup>, P. Zini<sup>30</sup>, F. Zomer<sup>28</sup>, J. Zsembery<sup>9</sup> and M. zurNedden<sup>38</sup>

<sup>1</sup> *I. Physikalisches Institut der RWTH, Aachen, Germany<sup>a</sup>*

<sup>2</sup> *III. Physikalisches Institut der RWTH, Aachen, Germany<sup>a</sup>*

<sup>3</sup> *School of Physics and Space Research, University of Birmingham, Birmingham, UK<sup>b</sup>*

<sup>4</sup> *Inter-University Institute for High Energies ULB-VUB, Brussels; Universitaire Instelling Antwerpen, Wilrijk; Belgium<sup>c</sup>*

<sup>5</sup> *Rutherford Appleton Laboratory, Chilton, Didcot, UK<sup>b</sup>*

<sup>6</sup> *Institute for Nuclear Physics, Cracow, Poland<sup>d</sup>*

<sup>7</sup> *Physics Department and IIRPA, University of California, Davis, California, USA<sup>e</sup>*

<sup>8</sup> *Institut für Physik, Universität Dortmund, Dortmund, Germany<sup>a</sup>*

<sup>9</sup> *DSM/DAPNIA, CEA/Saclay, Gif-sur-Yvette, France*

<sup>10</sup> *Department of Physics and Astronomy, University of Glasgow, Glasgow, UK<sup>b</sup>*

<sup>11</sup> *DESY, Hamburg, Germany<sup>a</sup>*

<sup>12</sup> *I. Institut für Experimentalphysik, Universität Hamburg, Hamburg, Germany<sup>a</sup>*

<sup>13</sup> *II. Institut für Experimentalphysik, Universität Hamburg, Hamburg, Germany<sup>a</sup>*

<sup>14</sup> *Max-Planck-Institut für Kernphysik, Heidelberg, Germany<sup>a</sup>*

<sup>15</sup> *Physikalisches Institut, Universität Heidelberg, Heidelberg, Germany<sup>a</sup>*

<sup>16</sup> *Institut für Hochenergiephysik, Universität Heidelberg, Heidelberg, Germany<sup>a</sup>*

<sup>17</sup> *Institut für Reine und Angewandte Kernphysik, Universität Kiel, Kiel, Germany<sup>a</sup>*

<sup>18</sup> *Institute of Experimental Physics, Slovak Academy of Sciences, Košice, Slovak Republic<sup>f,j</sup>*

<sup>19</sup> *School of Physics and Chemistry, University of Lancaster, Lancaster, UK<sup>b</sup>*

<sup>20</sup> *Department of Physics, University of Liverpool, Liverpool, UK<sup>b</sup>*

<sup>21</sup> *Queen Mary and Westfield College, London, UK<sup>b</sup>*

<sup>22</sup> *Physics Department, University of Lund, Lund, Sweden<sup>g</sup>*

<sup>23</sup> *Physics Department, University of Manchester, Manchester, UK<sup>b</sup>*

<sup>24</sup> *CPPM, Université d'Aix-Marseille II, IN2P3-CNRS, Marseille, France*

<sup>25</sup> *Institute for Theoretical and Experimental Physics, Moscow, Russia*

<sup>26</sup> *Lebedev Physical Institute, Moscow, Russia<sup>f</sup>*

<sup>27</sup> *Max-Planck-Institut für Physik, München, Germany<sup>a</sup>*

<sup>28</sup> *LAL, Université de Paris-Sud, IN2P3-CNRS, Orsay, France*

<sup>29</sup> *LPNHE, Ecole Polytechnique, IN2P3-CNRS, Palaiseau, France*

<sup>30</sup> *LPNHE, Universités Paris VI and VII, IN2P3-CNRS, Paris, France*

<sup>31</sup> *Institute of Physics, Czech Academy of Sciences, Praha, Czech Republic<sup>f,h</sup>*

- <sup>32</sup> *Nuclear Center, Charles University, Praha, Czech Republic<sup>f,h</sup>*  
<sup>33</sup> *INFN Roma 1 and Dipartimento di Fisica, Università Roma 3, Roma, Italy*  
<sup>34</sup> *Paul Scherrer Institut, Villigen, Switzerland*  
<sup>35</sup> *Fachbereich Physik, Bergische Universität Gesamthochschule Wuppertal, Wuppertal, Germany<sup>f</sup>*  
<sup>36</sup> *DESY, Institut für Hochenergiephysik, Zeuthen, Germany<sup>f</sup>*  
<sup>37</sup> *Institut für Teilchenphysik, ETH, Zürich, Switzerland<sup>i</sup>*  
<sup>38</sup> *Physik-Institut der Universität Zürich, Zürich, Switzerland<sup>i</sup>*  
<sup>39</sup> *Institut für Physik, Humboldt-Universität, Berlin, Germany<sup>f</sup>*  
<sup>40</sup> *Rechenzentrum, Bergische Universität Gesamthochschule Wuppertal, Wuppertal, Germany<sup>f</sup>*

<sup>a</sup> *Supported by the Bundesministerium für Bildung, Wissenschaft, Forschung und Technologie, FRG, under contract numbers 6AC17P, 6AC47P, 6DO57I, 6HH17P, 6HH27I, 6HD17I, 6HD27I, 6KI17P, 6MP17I, and 6WT87P*

<sup>b</sup> *Supported by the UK Particle Physics and Astronomy Research Council, and formerly by the UK Science and Engineering Research Council*

<sup>c</sup> *Supported by FNRS-NFWO, IISN-IKW*

<sup>d</sup> *Partially supported by the Polish State Committee for Scientific Research, grant no. 115/E-343/SPUB/P03/120/96*

<sup>e</sup> *Supported in part by USDOE grant DE F603 91ER40674*

<sup>f</sup> *Supported by the Deutsche Forschungsgemeinschaft*

<sup>g</sup> *Supported by the Swedish Natural Science Research Council*

<sup>h</sup> *Supported by GA ČR grant no. 202/96/0214, GA AV ČR grant no. A1010619 and GA UK grant no. 177*

<sup>i</sup> *Supported by the Swiss National Science Foundation*

<sup>j</sup> *Supported by VEGA SR grant no. 2/1325/96*

# 1 Introduction

Hadronic final states in deep inelastic  $ep \rightarrow e'X$  scattering (DIS neutral current interaction) offer an ideal environment to study hadronisation phenomena and to measure the strong coupling constant over a wide range of momentum transfer  $Q$  in a single experiment. Event shape variables have been investigated in  $e^+e^-$  experiments and used to extract the strong coupling constant  $\alpha_s(M_Z)$  independent of any jet algorithm, see *e.g.* ref. [1]. In deep inelastic scattering a similar analysis can be performed, provided the current (quark) fragmentation can be isolated from the target (proton remnant) fragmentation region. A particularly suitable frame of reference in which to study the current region with minimal contamination from target fragmentation effects is the Breit frame. Consider, for illustration, the quark parton model. In the Breit system the purely space-like gauge boson  $\gamma/Z$  with four-momentum  $q_{\gamma/Z} = \{0, 0, 0, -Q\}$  collides with the incoming quark with longitudinal momentum  $p_{qz}^{in} = Q/2$ . The outgoing quark is back-scattered into the current hemisphere with longitudinal momentum  $p_{qz}^{out} = -Q/2$ , while the proton fragments in the opposite hemisphere. The available energy for fragmentation in the Breit current hemisphere is  $Q/2$ . This situation can be compared with  $e^+e^- \rightarrow q\bar{q}$  annihilation, where the available energy in one hemisphere, *e.g.* defined by the thrust axis, is  $\sqrt{s_{ee}}/2$ . DIS event properties in the Breit current hemisphere should be similar and may be comparable to those in  $e^+e^-$  collisions at a scale  $Q = \sqrt{s_{ee}}$ .

In this paper an analysis of the event shape variables thrust, jet broadening and jet mass in the current hemisphere of the Breit frame in deep inelastic  $ep$  scattering is presented and compared with results from  $e^+e^-$  experiments. The kinematic phase space extends over  $7 \text{ GeV} < Q < 100 \text{ GeV}$  in momentum transfer and  $0.05 < y < 0.8$  in the kinematic variable  $y$ . Based on only recently available second order QCD calculations [2, 3] and on new developments in the treatment of non-perturbative hadronisation contributions to final states in deep inelastic scattering [4], the  $Q$  dependences of the mean event shape parameters are investigated to study simultaneously both the power, or hadronisation, corrections and the strong coupling constant  $\alpha_s(M_Z)$  independently of any fragmentation model.

## 2 Data Selection and Analysis Procedure

**The H1 Detector** Deep inelastic  $ep$  scattering events were collected with the H1 detector at HERA ( $E_e = 27.5 \text{ GeV}$ ,  $E_p = 820 \text{ GeV}$ ,  $\sqrt{s} = 300 \text{ GeV}$ ). The H1 detector is described elsewhere [5]; here only the components relevant for the present analysis are briefly recalled. Only calorimetric information is used to reconstruct electromagnetic and hadronic clusters. The event vertex and the direction of the scattered lepton are obtained with the tracking detectors.

The calorimeter system consists of a liquid argon (LAr) calorimeter, a backward calorimeter and a tail catcher (instrumented iron yoke). The LAr sampling calorimeter covers the polar angle<sup>1</sup> range  $4^\circ \leq \theta \leq 153^\circ$  and all azimuthal angles. It consists of a lead/argon electromagnetic section followed by a stainless steel/argon section for the measurement of hadronic energy. Electromagnetic energies are measured with a resolution of  $\sigma(E)/E \simeq 12\%/\sqrt{E} \oplus 1\%$  and hadronic energies with  $\sigma(E)/E \simeq 50\%/\sqrt{E} \oplus 2\%$ , as obtained from test beam results. The absolute energy scales are known to 3% and 4% for electrons and hadrons, respectively. A lead/scintillator electromagnetic backward calorimeter (BEMC) extends the coverage at large

---

<sup>1</sup>Polar angles  $\theta$  are defined with respect to the incident proton direction.

angles ( $155^\circ \leq \theta \leq 176^\circ$ ). The electromagnetic energy calibration is known to 1%. Since 1995 the backward region has been equipped with a lead/scintillating fibre calorimeter [6]. The instrumented iron flux return yoke is used to measure the leakage of hadronic showers.

Located inside the calorimeters is a tracking system, which consists of central drift and proportional chambers ( $25^\circ \leq \theta \leq 155^\circ$ ), a forward track detector ( $7^\circ \leq \theta \leq 25^\circ$ ) and a backward proportional chamber ( $155^\circ \leq \theta \leq 175^\circ$ ). In 1995 the latter was replaced by backward drift chambers. The tracking chambers and calorimeters are surrounded by a superconducting solenoid providing a uniform field of 1.15 T throughout the tracking volume.

The luminosity is determined from the rate of the Bethe–Heitler process  $ep \rightarrow ep\gamma$  measured in a luminosity monitor far downstream in the electron direction.

**Data Selection** The DIS data cover a large range of momentum transfer  $Q$  between 7 GeV and 100 GeV and are selected with the following criteria:

1. The energy of the isolated scattered lepton has to exceed  $E'_e > 10$  GeV.
2. The polar angle of the scattered lepton has to be within  $157^\circ < \theta_e < 173^\circ$  (low  $Q$  sample) or  $30^\circ < \theta_e < 150^\circ$  (high  $Q$  sample).
3. The hadronic energy clusters have to be well contained within the calorimeter acceptances  $5.7^\circ < \theta_h < 170^\circ$ .
4. There must be hadronic energy in the forward region ( $4^\circ < \theta < 15^\circ$ ) which is larger than 0.5 GeV in order to exclude diffractive events with large rapidity gaps.
5. The energy and longitudinal momenta must satisfy  $30 \text{ GeV} < \sum_i E_i (1 - \cos \theta_i) < 65 \text{ GeV}$ , where the sum extends over all energy clusters.
6. The total hadronic energy in the Breit current hemisphere has to exceed  $0.1 Q$ .
7. The kinematic variables  $y$  have to fulfill  $0.05 < y_e < 0.80$  (measured using the lepton) and  $0.05 < y_h$  (measured using the hadronic energy flow).

For the low  $Q$  event sample ( $Q = 7 - 10$  GeV, 1994 data with  $e^+$  beam, integrated luminosity  $\mathcal{L} \simeq 2.9 \text{ pb}^{-1}$ ) the lepton is detected in the BEMC. The lepton direction is measured using the event vertex and the backward proportional chamber in front of the calorimeter. For the high  $Q$  event sample ( $Q = 14 - 100$  GeV, 1994 – 1996 data with  $e^\pm$  beams,  $\mathcal{L} \simeq 11.7 \text{ pb}^{-1}$ ) the lepton is detected in the LAr calorimeter and its direction is taken from an associated track measured in the central tracking system.

The event selection criteria are chosen so as to ensure a good measurement of the final state and to provide a clean DIS data sample. Requirements 1, 2 and 7 assure that the kinematic quantities are well measured. The criterion 5 provides a good containment of the final state particles and rejects events with a hard photon radiated from the incoming lepton and together with the high  $y$  cut of requirement 7 suppresses photoproduction events with a misidentified lepton. Using tagged events, the photoproduction background is estimated to be about 3% in the low  $Q$  sample and to be negligible at high values of  $Q$ . To define shape variables, events are required to have hadronic activity in the Breit current hemisphere according to criterion 6.

**Analysis Procedure** The kinematic quantities needed to perform the Breit frame transformation, the negative squared momentum transfer  $Q^2$  and Bjorken  $x = Q^2/y s$ , are calculated from the scattered lepton ( $E'_e, \theta_e, \phi_e$ ) and hadron ( $E_h, \theta_h, \phi_h$ ) measurements using

$$Q^2 = 4 E_e E'_e \cos^2 \frac{\theta_e}{2}, \quad (1)$$

$$y \equiv y_e = 1 - \frac{E'_e}{E_e} \sin^2 \frac{\theta_e}{2} \quad \text{for } y_e > 0.15, \quad (2)$$

$$y \equiv y_h = \frac{\sum_h E_h (1 - \cos \theta_h)}{2 E_e} \quad \text{for } y_e < 0.15. \quad (3)$$

The momentum transfer  $Q^2$  is always best measured using the lepton. The kinematic variable  $y$  is taken from the lepton for sufficiently large values. However, since the resolution in  $y_e$  degrades severely at low values,  $y$  is determined using  $y_h$  if  $y_e < 0.15$ . This procedure ensures least uncertainty in the Lorentz transformation to the Breit frame.

The data are corrected for detector effects (acceptance, resolution, energy scale) using a full Monte Carlo simulation of the detector response. The Monte Carlo event selection and analysis are the same as for the data. The LEPTO event generator [7] including matrix elements plus parton showers is used over the full  $Q$  range. At low  $Q$ , however, events generated with ARIADNE [8] according to the colour dipole model are also included in order to enlarge the Monte Carlo statistics. Both simulations are based on the MRS H parton density parametrisations [9] and they describe the data well.

The observed differential event shape distributions  $\{F_i\}$  are corrected with a matrix method  $F_i^{cor} = \sum_j C_{ij} F_j^{data}$ . In principle the matrix  $\mathcal{C}$  may be obtained by an inversion of the matrix  $\mathcal{M}$  which transforms the ‘true’ values into observed values  $F_i^{obs} = \sum_j M_{ij} F_j^{true}$ , including the detector effects as described by a Monte Carlo simulation. In practice, however, the inversion of  $\mathcal{M}$  poses mathematical problems and leads to instabilities and oscillations, unless extremely large Monte Carlo statistics are available. Instead, the probability densities  $\rho_{ij}^{MC}$  correlating the observed and ‘true’ quantities, *i.e.*  $F_i^{true} = \sum_j \rho_{ij}^{MC} F_j^{obs}$ , are used to get the correction matrix  $C_{ij} = \rho_{ij}^{MC} / \sum_k \rho_{kj}^{MC}$ . This method may still have some model dependence, which could be overcome by an iterative procedure. However, as the data are described acceptably by the Monte Carlo simulations no iteration is performed.

Systematic uncertainties in the data analysis are evaluated for the mean values of the event shape variables, which are computed from the differential distributions. The following sources are considered: (i) the influence of the unfolding procedure, *i.e.* applying the matrix method or a bin-by-bin correction method; (ii) a variation of the energy scales, which affects the Breit frame transformation but has a small effect on the event shape parameters, since they involve ratios of hadronic momenta or energies; and (iii) the use of the HERWIG event generator [10] with fragmentation properties which are different from LEPTO. All contributions are of similar size over the whole range of  $Q$ . QED radiative corrections, which are studied with the DJANGO event generator [11], are found to have a negligible effect on the event shapes. The sum of all systematic errors of the mean event shape variables varies between  $\sim 2\%$  at low  $Q$  values and up to  $\sim 8\%$  at high  $Q$  values.

### 3 Event Shapes in the Breit Current Hemisphere

The infrared safe event shape variables thrust  $T_c$  and  $T_z$ , the jet broadening  $B_c$  and the jet mass  $\rho_c$  are studied in the Breit current hemisphere. The definitions of the event shape variables are given below, where the sums extend over all hadrons  $h$  (being a calorimetric cluster in the detector or a parton in the QCD calculations) with four-momentum  $p_h = \{E_h, \mathbf{p}_h\}$  fulfilling  $\cos(\mathbf{p}_h \cdot \mathbf{n}) > 0$ . The current hemisphere axis  $\mathbf{n} = \{0, 0, -1\}$  coincides with the virtual boson direction.

- **Thrust  $T_c$**

$$T_c = \max \frac{\sum_h |\mathbf{p}_h \cdot \mathbf{n}_T|}{\sum_h |\mathbf{p}_h|} \quad \mathbf{n}_T \equiv \text{thrust axis}, \quad (4)$$

- **Thrust  $T_z$**

$$T_z = \frac{\sum_h |\mathbf{p}_h \cdot \mathbf{n}|}{\sum_h |\mathbf{p}_h|} = \frac{\sum_h |\mathbf{p}_{zh}|}{\sum_h |\mathbf{p}_h|} \quad \mathbf{n} \equiv \text{hemisphere axis}, \quad (5)$$

- **Jet Broadening  $B_c$**

$$B_c = \frac{\sum_h |\mathbf{p}_h \times \mathbf{n}|}{2 \sum_h |\mathbf{p}_h|} = \frac{\sum_h |\mathbf{p}_{\perp h}|}{2 \sum_h |\mathbf{p}_h|} \quad \mathbf{n} \equiv \text{hemisphere axis}, \quad (6)$$

- **Jet Mass  $\rho_c$**

$$\rho_c = \frac{M^2}{Q^2} = \frac{(\sum_h p_h)^2}{Q^2}. \quad (7)$$

The normalized differential spectra of the event shape variables in the current hemisphere of the Breit frame and their mean values as a function of  $Q$  are presented in figs. 1 and 2. The mean values of the event shape parameters are also listed in table 1. They extend over a large range of momentum transfers  $Q$  between 7 GeV and 100 GeV. The corrected data, spectra and mean values, are well described by the LEPTO Monte Carlo generator for all  $Q$ .

A common characteristic of the event shape spectra of  $1 - T_c$ ,  $1 - T_z$ ,  $B_c$  and  $\rho_c$  is that they get narrower and more peaked towards lower values as  $Q$ , or the available energy in the Breit current hemisphere, increases. This means that the energy flow becomes more collimated along the event shape axis. This fact is also evident from the mean values of the event shape variables, which exhibit a clear decrease with rising  $Q$ .

The energy dependence of the mean thrust and jet masses of the H1 DIS  $ep$  data may be compared with available  $e^+e^-$  results [12] at the scale  $Q = \sqrt{s_{ee}}$ . Recall, however, that the event shape parameters in  $ep$  scattering are calculated in a single hemisphere, *i.e.* the current hemisphere of the Breit system, and that a ‘natural’ axis comparable with the virtual boson direction does not exist in  $e^+e^-$  annihilation. There, the virtual boson is at rest and the event axis is typically chosen to be the thrust axis.

The  $Q$  dependence of the means  $\langle 1 - T_c \rangle$  in fig. 2a is in qualitative agreement with the  $e^+e^-$  measurements. However, the  $e^+e^-$  data points, coming from many experiments, tend



to lie systematically above the  $ep$  data at low values of  $Q \lesssim 15$  GeV. This can be partially understood from the fact that in  $e^+e^-$  experiments thrust is calculated for the whole event and not in a single hemisphere, which tends to deplete the high thrust region. This property is also demonstrated by comparing the thrust spectra of fig. 1a with the corresponding distributions at similar energies of the PLUTO and TASSO experiments [12]. Furthermore, from the definition of eq. (4), it can be seen that thrust  $T_c$  measures a mixture of the longitudinal and transverse momentum components with respect to the boson direction. In strongly collimated events the thrust axis is close to the  $\gamma/Z$  axis and  $T_c$  is essentially given by the longitudinal momenta. However, for more isotropic events, which frequently occur at low  $Q$ , the thrust axis flips by up to  $90^\circ$  and  $T_c$  is dominated by transverse momenta, resulting in higher thrust values and thus mimicking jet-like event configurations. Such a situation does not occur in  $e^+e^-$  analyses. The thrust definition  $T_z$  of eq. (5) is expected to be closer to the  $e^+e^-$  case. Indeed, with a proper rescaling in order to cover the same thrust range, the mean values  $\langle 1 - T_z \rangle / 2$  exhibit a stronger  $Q$  dependence, see fig. 2b, and are comparable to  $\langle 1 - T_{ee} \rangle$  at  $Q \lesssim 50$  GeV.

The mean jet masses  $\langle \rho_c \rangle$  in fig. 2d show a weaker  $Q$  dependence for  $ep$  scattering than for  $e^+e^-$  collisions, where the average of the heavy and light jet masses of both event hemispheres are plotted. The  $ep$  data are systematically higher at larger values of  $Q \gtrsim 20$  GeV. A possible explanation is the normalisation of  $\rho_c$  to  $Q^2$  in eq. (7). In the Breit current hemisphere multiparton final states tend to produce visible energy  $E_{vis} > Q/2$ , which is different from the quark parton model expectation and from the situation in  $e^+e^-$  annihilation. Indeed, a normalisation to  $4E_{vis}^2$  instead of  $Q^2$  gives better agreement between  $ep$  and  $e^+e^-$  data, particularly at high values of  $Q$ .

As argued above, one does not expect the event shapes distribution in deep inelastic  $ep$  scattering to correspond exactly to those for  $e^+e^-$  annihilation. There are other differences, which are not related to the analysis method. The  $e^+e^-$  data contain a considerably larger fraction of bottom quarks with different fragmentation properties than the light quarks, which may be important close to threshold energies. Furthermore, there are additional  $\mathcal{O}(\alpha_s)$  processes in deep inelastic scattering. Besides the common final state gluon radiation off quarks, in DIS there are contributions from initial state gluon radiation and boson gluon fusion.

## 4 QCD Calculations and Power Corrections

**Theoretical Framework** Any  $Q$  or energy dependence of the event shape variables can have the following origins: (i) the logarithmic change of the strong coupling constant  $\alpha_s(Q) \propto 1/\ln Q$ , and (ii) power corrections or hadronisation effects, which are expected to behave like  $1/Q$ . Recent theoretical developments suggest that  $1/Q$  corrections are not necessarily related to hadronisation, but may instead be a universal soft gluon phenomenon associated with the behaviour of the running coupling at small momentum scales [4, 13]. ‘Universal’ means that they could be expressible in terms of a few non-perturbative parameters with calculable process-dependent coefficients. The event shape data will now be analyzed by applying this approach which relates hadronisation effects in the final state observables to power corrections.

The mean value of any infrared safe event shape variable  $\langle F \rangle$  at a scale  $\mu_R$ , taken to be  $\mu_R = Q$ , can be written according to ref. [4] as

$$\langle F \rangle = \langle F \rangle^{\text{pert}} + \langle F \rangle^{\text{pow}} , \quad (8)$$

$$\langle F \rangle^{\text{pert}} = c_1 \alpha_s(\mu_R) + \left( c_2 + \frac{\beta_0}{2\pi} \ln \frac{\mu_R}{Q} c_1 \right) \alpha_s^2(\mu_R), \quad (9)$$

$$\langle F \rangle^{\text{pow}} = a_F \frac{16}{3\pi} \frac{\mu_I}{\mu_R} \ln^p \frac{\mu_R}{\mu_I} \left[ \bar{\alpha}_0(\mu_I) - \alpha_s(\mu_R) - \frac{\beta_0}{2\pi} \left( \ln \frac{\mu_R}{\mu_I} + \frac{K}{\beta_0} + 1 \right) \alpha_s^2(\mu_R) \right], \quad (10)$$

where  $\beta_0 = 11 - 2/3 N_f$ ,  $K = 67/6 - \pi^2/2 - 5/9 N_f$  and  $N_f = 5$  flavours.

The perturbative part, eq. (9), represents the second order QCD prediction, where the coefficients  $c_1$  and  $c_2$  are calculated in the  $\overline{\text{MS}}$  scheme at the scale  $\mu_R = Q$ . The power corrections, eq. (10) with coefficients  $a_F$  and  $p$  ( $p = 0$ , except  $p = 1$  for  $\langle B_c \rangle$ ) depending on the observable  $F$ , contain a free non-perturbative parameter  $\bar{\alpha}_0(\mu_I)$  to be evaluated at some ‘infrared matching’ scale  $\Lambda_{QCD} \ll \mu_I \ll \mu_R$ , conventionally chosen to be  $\mu_I = 2$  GeV. The parameter  $\bar{\alpha}_0(\mu_I)$  can be interpreted as an effective strong coupling constant below the matching scale  $\mu_I$ , calculated in leading order. The dependence on  $\mu_I$  is partially compensated by the  $\mu_I$  dependence of the other terms in eq. (10). The dependence on the renormalisation scale  $\mu_R$  should help to compensate the scale dependence of the perturbative part. The power corrections are expected to behave like  $1/\mu_R$  (*i.e.*  $p = 0$ ) for the event shape variables discussed in this paper, except for the jet broadening which is supposed to have an additional  $\ln(\mu_R/\mu_I)$  term (*i.e.*  $p = 1$ ). However, the prediction for  $\langle B_c \rangle$  is considered to be less reliable [4]. In this approach the data can be directly used to determine in a simultaneous fit the power correction parameters  $\bar{\alpha}_0(\mu_I)$  and the strong coupling constant  $\alpha_s(M_Z)$  without assuming any fragmentation model.

**Perturbative Predictions** In deep inelastic scattering the perturbative part, eq. (9), may be obtained via

$$\langle F \rangle^{\text{pert}} = \frac{\int_0^{F_{\text{max}}} F \frac{d\sigma}{dF} dF}{\int_0^{F_{\text{max}}} \frac{d\sigma}{dF} dF} = \frac{1}{\sigma_{\text{tot}}} \int_0^{F_{\text{max}}} F \frac{d\sigma}{dF} dF. \quad (11)$$

To get  $\langle F \rangle^{\text{pert}}$  to  $\mathcal{O}(\alpha_s^2)$  the Taylor expansion of eq. (11) shows that the integral in the numerator has to be evaluated in second order QCD, whereas the total cross section  $\sigma_{\text{tot}}$  needs only be known to first order, because the numerator vanishes,  $F \equiv 0$ , in the quark parton model.

The perturbative calculations can be performed with the MEPJET [2] and DISENT [3] programs. Both programs treat deep inelastic  $ep$  scattering to  $\mathcal{O}(\alpha_s^2)$  via single  $\gamma$  exchange. The neglect of  $Z$  exchange has no influence on event shape parameters in the range of  $Q$  investigated. The lack of virtual two-loop diagrams, however, leads to the restriction that  $\sigma_{\text{tot}}$  can only be calculated to  $\mathcal{O}(\alpha_s)$ , which, as explained above, is sufficient for the present analysis.

MEPJET applies the so-called ‘phase space slicing method’ for the integration. The real emission of partons (quarks, antiquarks and gluons) is calculated exactly for a two-parton resolution parameter  $s_{ij} > s_{\text{min}}$ , the invariant mass squared, with typical values of  $s_{\text{min}} \sim 0.01$  GeV<sup>2</sup>. Soft and collinear approximations are used in the region where at least one parton pair has  $s_{ij} < s_{\text{min}}$ . The final state infrared and collinear divergences cancel against virtual loop and tree diagrams. The cut on  $s_{\text{min}}$  prevents the integration of the event shape distributions  $F d\sigma/dF$  being carried out over the whole phase space. Instead, a lower bound  $F_{\text{cut}} > 0$ , which depends on the event shape under consideration, has to be imposed.

DISENT uses the ‘subtraction method’ and applies dipole factorisation formulae for the same set of  $\mathcal{O}(\alpha_s^2)$  diagrams. Since no  $s_{\text{min}}$  cut is needed and special care has been taken

concerning the numerical integration of  $F d\sigma/dF$ , which still contains integrable singularities, one is allowed to use the complete phase space  $0 \leq F \leq F_{\max}$ . Therefore the DISSENT results are applied throughout the present analysis. In the overlapping phase space regions with  $F > F_{\text{cut}}$  the differential event shape distributions of MEPJET and DISSENT agree very well and the mean values from both programs yield compatible results to within the statistical accuracy, which is less than 1% in first order and about 3% in second order perturbative QCD.

Fig. 3 shows the differential event shape spectra at the parton level based on the second order QCD calculations in comparison with the data. The lepton and partons are selected in the same way as in the data by requiring the criteria 1, 2, 6 and 7 of section 2. One clearly sees the strong impact of hadronisation effects, particularly at low values of  $Q$ . Towards higher values of  $Q$  the hadronisation becomes less important and the data and parton distributions approach each other. It is a consequence of the concept of ref. [4] that the mean values of the event shape spectra of the observed data and of the partons can be related by a single power correction parameter  $\bar{\alpha}_0$ .

For each event shape variable the coefficients  $c_1$  and  $c_2$  are obtained from a fit of eq. (9) to the  $Q$  dependence of the mean values, which themselves are calculated with DISSENT from eq. (11). The theoretical calculations are performed by using the MRS H parton distributions [9] and the corresponding value of the strong coupling constant. The coefficients  $c_1$ ,  $c_2$  of the perturbative part, eq. (9), and the coefficient  $a_F$  [4] of the power corrections, eq. (10), which are used in the following QCD analysis of the event shape variables are given in table 2.

**QCD Fits** Fits to the data of fig. 2 and table 1 show that contributions from second order power corrections  $\propto 1/Q^2$  are not required by the data. Such terms may occur because of higher-twist corrections and would be sensitive to the low  $Q$  measurements. All event shape variables can be well described by first order power corrections  $\propto 1/Q$  and an exponent  $p = 0$  for the logarithmic term.

Note that the power corrections for the jet broadening are expected to have a  $Q$  dependence different from the other event shapes variables. However, the ansatz  $\langle B_c \rangle^{\text{pow}} \propto 1/\mu_R \ln(\mu_R/\mu_I)$  of eq. (10) cannot be supported by the data. The additional logarithmic term varies by a factor of  $\sim 2.7$  and leads to a less steep  $Q$  dependence, resulting in an unacceptable fit. A modification of the logarithmic term to  $\ln(\mu_R/\mu_0)$  with  $\mu_0$  treated as a free parameter also does not give a satisfactory solution. Therefore this logarithmic term is discarded in the following analysis. This observation disagrees with the conjectured  $Q$  behaviour of ref. [4].

The results of the QCD analysis, assuming  $\mu_R = Q$  and  $\mu_I = 2$  GeV, are shown in fig. 4. The data are well represented by the fits to eqs. (8) – (10). The second order perturbative QCD predictions are also shown. The power corrections, or hadronisation contributions, are substantial at low values of  $Q$ , but become less important with increasing energy. A comparison with the corresponding LEPTO curves of fig. 2 shows that this event generator adequately describes the experimental data. However, the LEPTO parton level distributions look very different to the DISSENT or MEPJET calculations.

Theoretical uncertainties in the determination of  $\alpha_s(M_Z)$  and  $\bar{\alpha}_0$  come from the accuracy of the QCD calculations and from the choice of different possible scales. Varying the anti-correlated coefficients  $c_1$  and  $c_2$  of eq. (9) within their errors leads to typical changes of  $\delta\alpha_s^{\text{calc}} = \pm 0.001$  and  $\delta\bar{\alpha}_0^{\text{calc}} = \pm 0.002$ . Using a different parton density parametrisation would give negligible changes to  $\alpha_s$  and  $\bar{\alpha}_0$ . The separation between the non-perturbative and perturbative

contributions is characterized by the infrared matching scale  $\mu_I$  and the renormalisation scale  $\mu_R$ , which should satisfy the relation  $\Lambda \ll \mu_I \ll \mu_R$ . Requiring the criterion  $\mu_R/\mu_I > 3$  implies  $\mu_I < 2.5$  GeV if  $\mu_R = Q$  and  $\mu_R > 0.8Q$  if  $\mu_I = 2$  GeV. The upper value of the renormalisation scale is chosen such that the fitted  $\chi^2$  varies by about the same amount as for the statistical error determination, typically  $\mu_R < 1.5Q$ . A variation of the renormalisation scale within  $0.8Q < \mu_R < 1.5Q$  results in shifts of the order of  $\delta\alpha_s^{\mu_R} = \begin{smallmatrix} +0.005 \\ -0.004 \end{smallmatrix}$  and  $\delta\bar{\alpha}_0^{\mu_R} = \pm 0.05$ . The range of the infrared matching scale is chosen to be symmetric,  $\mu_I = 2.0 \pm 0.5$  GeV, which leads to typical changes of  $\delta\alpha_s^{\mu_I} = \pm 0.002$ , while the power corrections are proportional to  $\mu_I$ . All the theoretical uncertainties are added in quadrature.

## 5 Results of QCD Analysis

The final results for the power correction parameters  $\bar{\alpha}_0$  and the strong coupling constant  $\alpha_s(M_Z)$  in the  $\overline{\text{MS}}$  scheme are compiled in table 3. Note that the overall errors are dominated by systematic effects associated with the theory. The largest contribution comes from the renormalisation scale dependence, which could be reduced once  $\mathcal{O}(\alpha_s^3)$  calculations become available. However, there remains the interplay between the non-perturbative and perturbative regions. An effective means to get a larger separation between the renormalisation and the infrared matching scales would be to select data at higher values of  $Q$  at the expense of a lower sensitivity to both the power correction parameter and the strong coupling constant.

All event shape analyses give results consistent with each other for  $\bar{\alpha}_0$  and  $\alpha_s(M_Z)$ . It should be noted that the fitted parameters  $\bar{\alpha}_0$  are correlated with the preferred value of  $\alpha_s(M_Z)$ . The correlation coefficients change sign and magnitude for the various event shape variables.

It is particularly remarkable that the power correction parameters  $\bar{\alpha}_0$  of the event shapes under study are all of the same size to within  $\pm 15\%$ . The individual values are consistent with being universal and clearly support the concept and computations of ref. [4] of power corrections to the mean hadronic event shapes in deep inelastic  $ep$  scattering. It is notable, however, that the power correction parameter for the jet broadening is slightly lower than those of the other event shapes, which may be an indication that the adopted parametrisation is not completely correct, as noted in section 4.

The  $\alpha_s(M_Z)$  values show a larger spread than expected from the experimental errors alone. They become compatible with each other only if the theoretical uncertainties are taken into account. This indicates the importance of the influence of higher order QCD corrections, which may affect each event shape variable differently. A similar situation was observed in  $\mathcal{O}(\alpha_s^2)$  event shape analyses performed by  $e^+e^-$  experiments at LEP, see *e.g.* discussion in ref. [1].

An important result is the  $1/Q$  dependence of the power corrections to the mean event shape variables. The similarity of the  $\bar{\alpha}_0$  values suggests that the assumption of universal power corrections may be further tested by performing a common two-parameter fit to both thrust and the jet mass data, each of which exploits a different event shape property. The jet broadening data are neglected because of the arguments given above. In the common fit no account is taken for possible correlations between the event shape variables. The correlation between  $\bar{\alpha}_0$  and  $\alpha_s(M_Z)$  is much less than in the individual fits. The common fit (see table 3) gives a relatively large  $\chi^2/\text{ndf} \simeq 2$ , a possible reason being the missing higher order QCD corrections. The results of the fit are  $\bar{\alpha}_0 = 0.491 \pm 0.003$  (exp)  $\begin{smallmatrix} +0.079 \\ -0.042 \end{smallmatrix}$  (theory) for the power correction parameter and  $\alpha_s(M_Z) = 0.118 \pm 0.001$  (exp)  $\begin{smallmatrix} +0.007 \\ -0.006 \end{smallmatrix}$  (theory) for the strong coupling constant in the  $\overline{\text{MS}}$

scheme, where the experimental errors are determined from the  $\chi^2$  contour. It is clear from the sizes of the experimental and theoretical uncertainties that a better understanding of higher order QCD corrections to the event shape variables is necessary for further improvements.

From fits to the energy dependence ( $Q = \sqrt{s}$ ) of thrust  $\langle 1 - T_{ee} \rangle$  and the heavy jet mass  $\langle M_H^2/s \rangle$  of  $e^+e^-$  data [12], and using the the same approach with the QCD prescriptions of ref. [13], one obtains values for the power correction parameters which are consistent with the  $ep$  analyses, see table 3. In a similar analysis with a different choice of  $e^+e^-$  experiments DELPHI [12] finds consistent results, but a slightly smaller value of  $\alpha_s(M_Z)$  for the thrust variable. These observations suggest that the power correction parameters  $\bar{\alpha}_0$  are universal to within  $\sim 20\%$  in both deep inelastic  $ep$  scattering and  $e^+e^-$  annihilation.<sup>2</sup>

## 6 Conclusion

The event shape variables thrust, jet broadening and jet mass are studied for the first time in the current hemisphere of the Breit frame in deep inelastic  $ep$  scattering. Differential distributions and mean values are measured over a wide range of momentum transfers  $Q$  from 7 GeV to 100 GeV. The mean values of the event shapes exhibit a strong  $Q$  dependence. They decrease with rising  $Q$ , *i.e.* the energy flow in the Breit current hemisphere becomes more collimated. The means of thrust and jet mass show a similar energy dependence to that measured in  $e^+e^-$  annihilation at the scale  $Q = \sqrt{s_{ee}}$ . Differences can be plausibly attributed to the different QCD dynamics for, and to the analysis methods which are applied to,  $ep$  and  $e^+e^-$  scattering.

Using  $\mathcal{O}(\alpha_s^2)$  QCD calculations and a specific model to describe the influence of non-perturbative effects on hadronic final states, the  $Q$  dependences of the mean event shape parameters are fitted to determine simultaneously the power or hadronisation corrections and the strong coupling constant  $\alpha_s(M_Z)$  in the  $\overline{\text{MS}}$  scheme without assuming any fragmentation model. The power corrections decrease with the expected power of  $1/Q$  and can be described by a common universal parameter  $\bar{\alpha}_0$  which is consistent with the values found in  $e^+e^-$  experiments. However, the conjectured  $1/Q \ln Q$  dependence of the jet broadening power corrections cannot be supported by the  $ep$  data. The present precision of both the power correction parameters and the strong coupling constant is limited by theoretical uncertainties due to unknown higher order QCD corrections, which are to some extent accounted for by a variation of the renormalisation and infrared matching scales.

**Acknowledgments** We are grateful to the HERA machine group whose outstanding efforts have made and continue to make this experiment possible. We thank the engineers and technicians for their work in constructing and now maintaining the H1 detector, our funding agencies for financial support, the DESY technical staff for continual assistance, and the DESY directorate for the hospitality which they extend to the non-DESY members of the collaboration. We gratefully acknowledge valuable discussions with E. Mirkes, M. Seymour and B.R. Webber.

---

<sup>2</sup>Notice that any analysis of the mean event shape variables in  $e^+e^-$  experiments also suffers from missing higher order QCD corrections.

## References

- [1] S. Bethke, Proceedings *QCD 94*, Montpellier, ed. S Narison, Nucl. Phys. B (Proc. Suppl.) 39 B, C (1995), p. 198.
- [2] E. Mirkes and D. Zeppenfeld, Phys. Lett. B 380 (1996) 205 and hep-ph/9511448; E. Mirkes, private communication.
- [3] S. Catani and M. Seymour, Nucl. Phys. B 485 (1997) 291 and hep-ph/9605323; M. Seymour, private communication.
- [4] B.R. Webber, Proceedings *Workshop on Deep Inelastic Scattering and QCD*, Paris (1995), eds. J.F. Laporte and Y. Sirois, p. 115; B.R. Webber, private communication; M. Dasgupta and B.R. Webber, preprint Cavendish-HEP-96/5 and hep-ph/9704297.
- [5] H1 Collaboration, I. Abt et al., Nucl. Instr. and Meth. A 386 (1997) 310 and Nucl. Instr. and Meth. A 386 (1997) 348.
- [6] H1 SpaCal Group, R.D. Appuhn et al., DESY report 96-171 (1996), to be published in Nucl. Instr. and Meth. A.
- [7] G. Ingelman, Proceedings *Physics at HERA*, Hamburg (1991), eds. W. Buchmüller and G. Ingelman, vol. 3, p. 1366.
- [8] L. Lönnblad, Computer Phys. Comm. 71 (1992) 15.
- [9] A.D. Martin, W.J. Stirling and R.G. Roberts, Proceedings *Workshop on Quantum Field Theory and Theoretical Aspects of High Energy Physics* (1993), eds. B. Geyer and E.M. Ilgenfritz, p. 11.
- [10] G. Marchesini et al., Computer Phys. Comm. 67 (1992) 465.
- [11] G.A. Schuler and H. Spiesberger, Proceedings *Physics at HERA*, Hamburg (1991), eds. W. Buchmüller and G. Ingelman, vol. 3, p. 1419.
- [12] PLUTO Collaboration, Ch. Berger et al., Z. Phys. C 12 (1982) 297;  
Mark II Collaboration, A. Peterson et al., Phys. Rev. D 37 (1988) 1;  
TASSO Collaboration, W. Braunschweig et al., Z. Phys. C 45 (1989) 11 and Z. Phys. C 47 (1990) 187;  
AMY Collaboration, Y.K. Li et al., Phys. Rev. D 41 (1990) 2675;  
DELPHI Collaboration, P. Abreu et al., Z. Phys. C 73 (1997) 229.
- [13] Yu.L. Dokshitzer and B.R. Webber, Phys. Lett. B 352 (1995) 451;  
Z. Kunszt, P. Nason, G. Marchesini and B.R. Webber, *Z Physics at LEP 1*, eds. G. Altarelli, R. Kleiss and C. Verzegnassi, CERN 89-08, vol. 1, p. 373.

$\langle Q \rangle$ [GeV]	$\langle 1 - T_c \rangle$	$\langle Q \rangle$ [GeV]	$\langle 1 - T_z \rangle / 2$
7.47	$0.1678 \pm 0.0019 \pm 0.0023$	7.47	$0.2182 \pm 0.0019 \pm 0.0024$
8.91	$0.1631 \pm 0.0021 \pm 0.0019$	8.91	$0.2009 \pm 0.0022 \pm 0.0023$
14.9	$0.1251 \pm 0.0016 \pm 0.0021$	14.9	$0.1555 \pm 0.0018 \pm 0.0023$
17.8	$0.1193 \pm 0.0012 \pm 0.0022$	17.8	$0.1351 \pm 0.0014 \pm 0.0025$
24.2	$0.1072 \pm 0.0012 \pm 0.0025$	24.2	$0.1125 \pm 0.0013 \pm 0.0024$
37.9	$0.0880 \pm 0.0018 \pm 0.0021$	37.9	$0.0912 \pm 0.0019 \pm 0.0023$
68.0	$0.0746 \pm 0.0037 \pm 0.0023$	68.0	$0.0635 \pm 0.0035 \pm 0.0049$

$\langle Q \rangle$ [GeV]	$\langle B_c \rangle$	$\langle Q \rangle$ [GeV]	$\langle \rho_c \rangle$
7.47	$0.3566 \pm 0.0019 \pm 0.0071$	7.47	$0.1055 \pm 0.0015 \pm 0.0023$
8.91	$0.3414 \pm 0.0023 \pm 0.0076$	8.91	$0.1009 \pm 0.0015 \pm 0.0024$
14.9	$0.2978 \pm 0.0018 \pm 0.0069$	14.9	$0.0871 \pm 0.0010 \pm 0.0031$
17.8	$0.2704 \pm 0.0013 \pm 0.0067$	17.8	$0.0816 \pm 0.0008 \pm 0.0020$
24.2	$0.2394 \pm 0.0014 \pm 0.0070$	24.2	$0.0780 \pm 0.0008 \pm 0.0030$
37.9	$0.2039 \pm 0.0023 \pm 0.0093$	37.9	$0.0637 \pm 0.0013 \pm 0.0030$
68.0	$0.1654 \pm 0.0046 \pm 0.0107$	68.0	$0.0512 \pm 0.0024 \pm 0.0021$

Table 1: Mean values of the event shape variables thrust  $\langle 1 - T_c \rangle$  and  $\langle 1 - T_z \rangle / 2$ , jet broadening  $\langle B_c \rangle$  and jet mass  $\langle \rho_c \rangle$  as a function of  $Q$ . The first error is statistical, the second systematic

Observable	$c_1$	$c_2$	$a_F$
$\langle 1 - T_c \rangle$	$0.384 \pm 0.033$	$0.57 \pm 0.21$	1
$\langle 1 - T_z \rangle / 2$	$0.053 \pm 0.033$	$3.45 \pm 0.23$	1
$\langle B_c \rangle$	$0.990 \pm 0.121$	$2.39 \pm 0.86$	2
$\langle \rho_c \rangle$	$0.359 \pm 0.048$	$-0.05 \pm 0.30$	1/2

Table 2: Coefficients  $c_1$ ,  $c_2$  and  $a_F$  of the event shape variables used in the QCD fits

Observable	$\bar{\alpha}_0(\mu_I = 2 \text{ GeV})$	$\alpha_s(M_Z)$	$\chi^2/\text{ndf}$
H1 $ep$ data			
$\langle 1 - T_c \rangle$	$0.497 \pm 0.005$ $^{+0.070}_{-0.036}$	$0.123 \pm 0.002$ $^{+0.007}_{-0.005}$	5.0/5
$\langle 1 - T_z \rangle / 2$	$0.507 \pm 0.008$ $^{+0.109}_{-0.051}$	$0.115 \pm 0.002$ $^{+0.007}_{-0.005}$	8.5/5
$\langle B_c \rangle$	$0.408 \pm 0.006$ $^{+0.036}_{-0.022}$	$0.119 \pm 0.003$ $^{+0.007}_{-0.004}$	5.3/5
$\langle \rho_c \rangle$	$0.519 \pm 0.009$ $^{+0.025}_{-0.020}$	$0.130 \pm 0.003$ $^{+0.007}_{-0.005}$	3.1/5
common fit			
$T_c, T_z, \rho_c$	$0.491 \pm 0.003$ $^{+0.079}_{-0.042}$	$0.118 \pm 0.001$ $^{+0.007}_{-0.006}$	39/19
$e^+e^-$ data			
$\langle 1 - T_{ee} \rangle$	$0.519 \pm 0.009$ $^{+0.093}_{-0.039}$	$0.123 \pm 0.001$ $^{+0.007}_{-0.004}$	10.9/14
$\langle M_H^2/s \rangle$	$0.431 \pm 0.020$ $^{+0.071}_{-0.030}$	$0.115 \pm 0.002$ $^{+0.005}_{-0.003}$	7.8/14

Table 3: Results on power correction parameters  $\bar{\alpha}_0$  and the strong coupling constant  $\alpha_s(M_Z)$  from fits to the  $Q$  dependence of the mean event shape variables. In the common fit possible correlations between the event shape variables are not taken into account. The first error is experimental, the second error represents theoretical uncertainties. The  $e^+e^-$  experiments [12] use the heavy jet mass  $M_H$



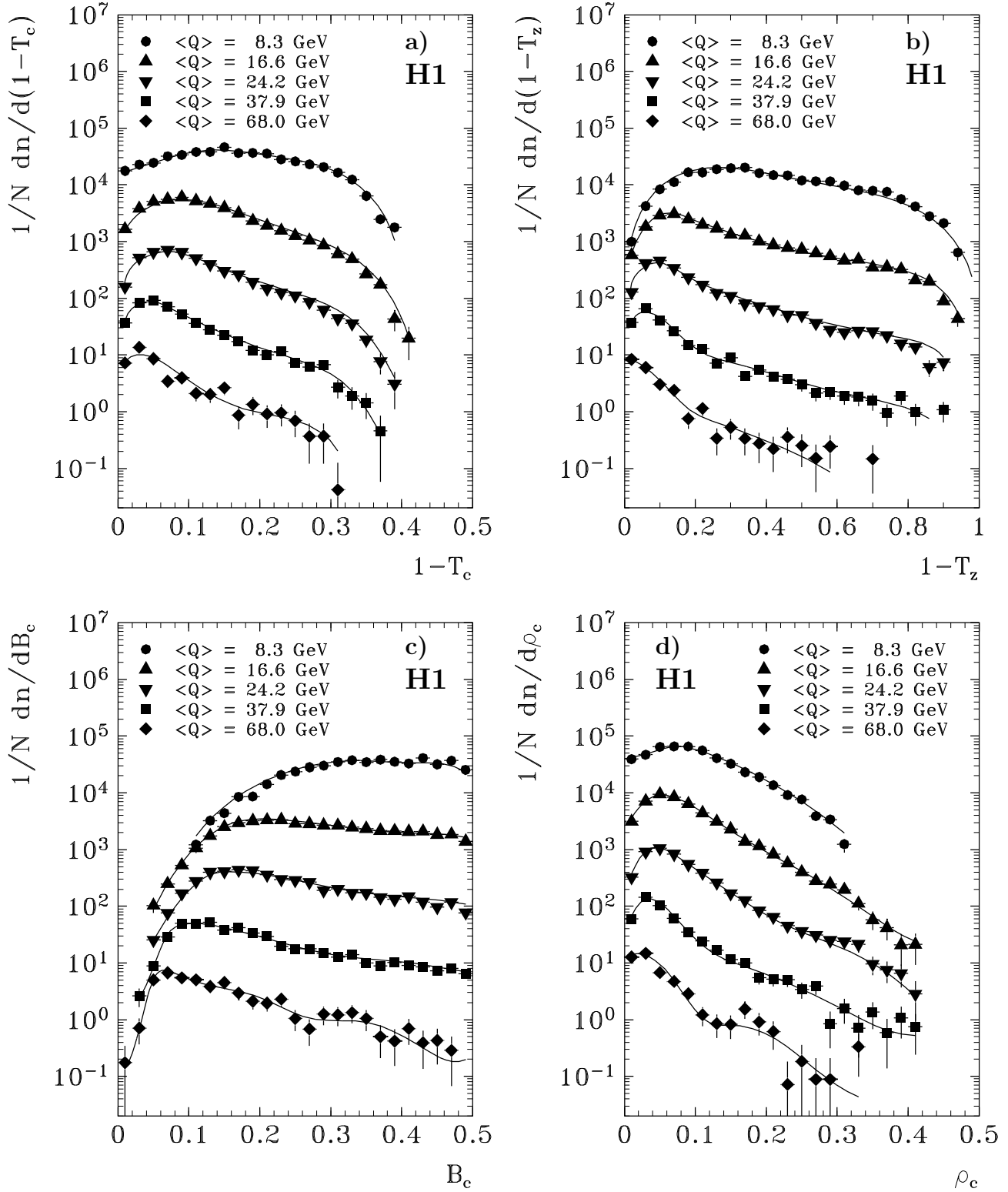


Figure 1: Differential event shape distributions of **a)** thrust  $1/N dn/d(1 - T_c)$ , **b)** thrust  $1/N dn/d(1 - T_z)$ , **c)** jet broadening  $1/N dn/dB_c$  and **d)** jet mass  $1/N dn/d\rho_c$ . H1 DIS  $ep$  data (full symbols, only statistical errors shown) are compared with LEPTO Monte Carlo simulations (—). The spectra for  $\langle Q \rangle = 8.3 - 68$  GeV are multiplied by factors of  $10^n$  ( $n = 0, 4$ )

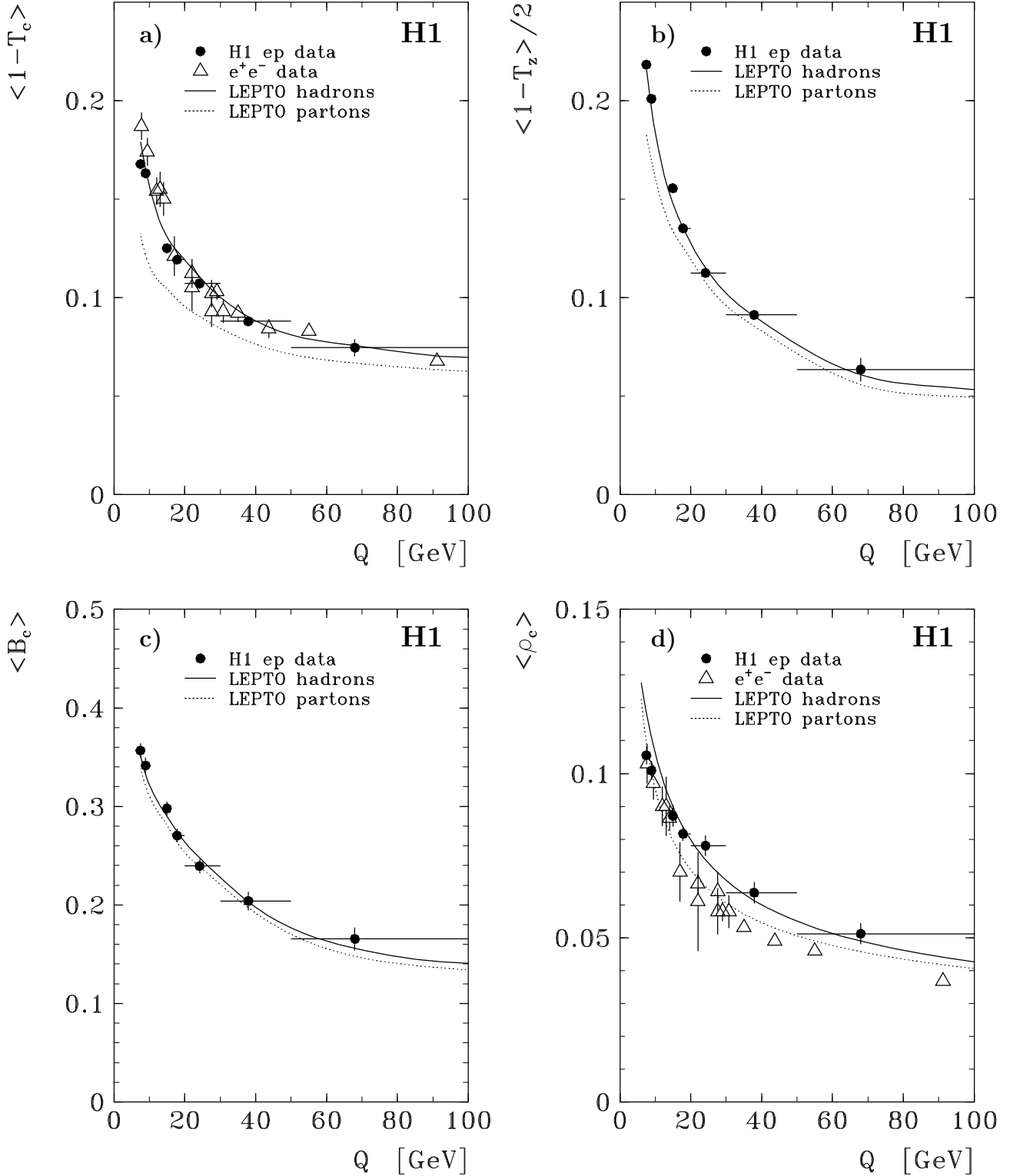


Figure 2: Mean event shape variables as a function of  $Q$  for **a)**  $\langle 1 - T_c \rangle$ , **b)**  $\langle 1 - T_z \rangle / 2$ , **c)**  $\langle B_c \rangle$ , and **d)**  $\langle \rho_c \rangle$ . H1 DIS  $ep$  data ( $\bullet$ , errors include statistics and systematics) are compared with LEPTO Monte Carlo simulations for hadrons (—) and partons ( $\cdots$ ). Data from  $e^+e^-$  experiments ( $\triangle$ ) are shown for thrust  $\langle 1 - T_{ee} \rangle$ , calculated for the whole event, and for the average of the heavy and light jet masses

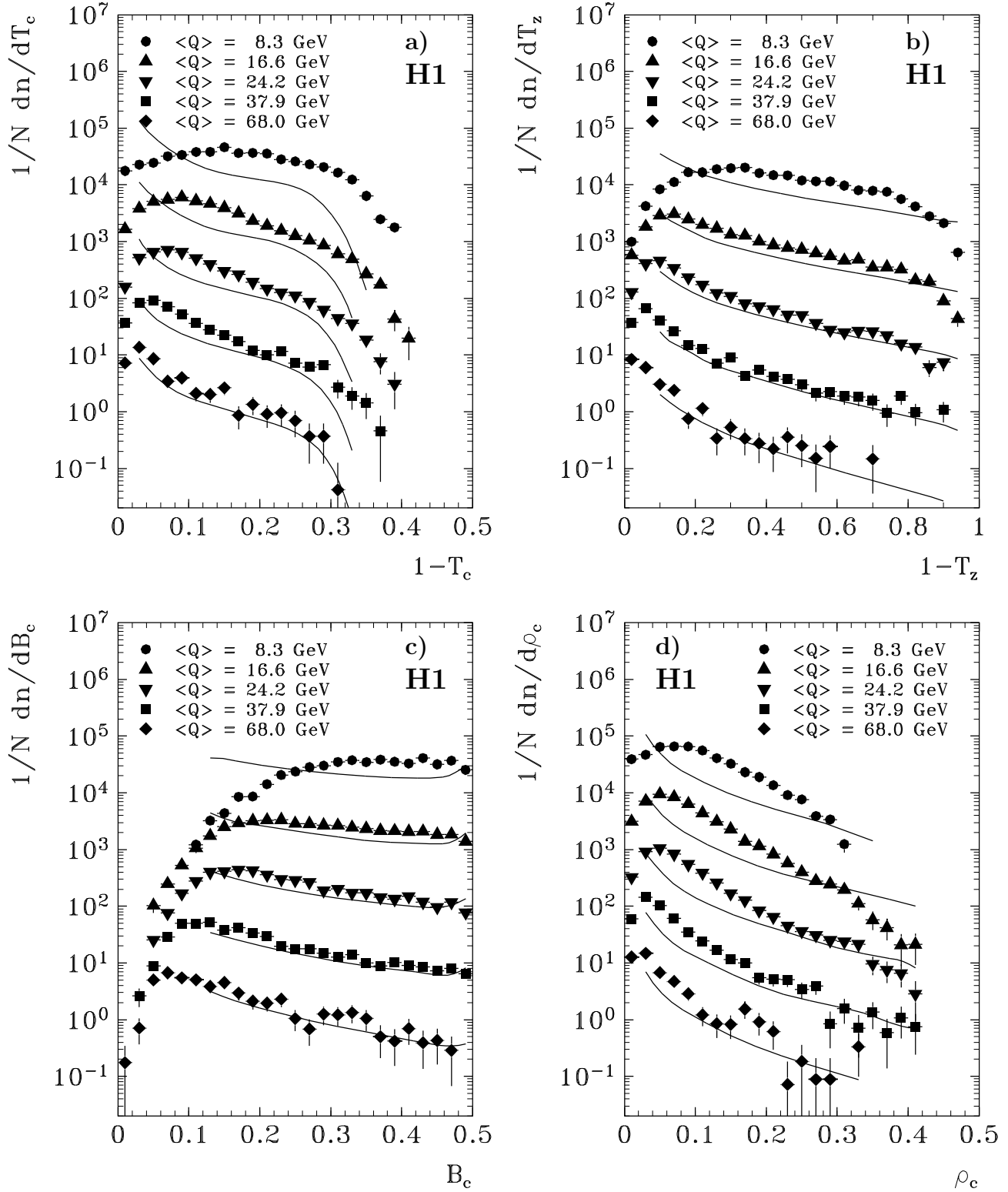


Figure 3: Differential event shape distributions of **a)** thrust  $1/N dn/d(1 - T_c)$ , **b)** thrust  $1/N dn/d(1 - T_z)$ , **c)** jet broadening  $1/N dn/dB_c$  and **d)** jet mass  $1/N dn/d\rho_c$ . H1 DIS  $ep$  data (full symbols, only statistical errors shown) are compared with second order QCD calculations (—). The spectra for  $\langle Q \rangle = 8.3 - 68$  GeV are multiplied by factors of  $10^n$  ( $n = 0, 4$ )

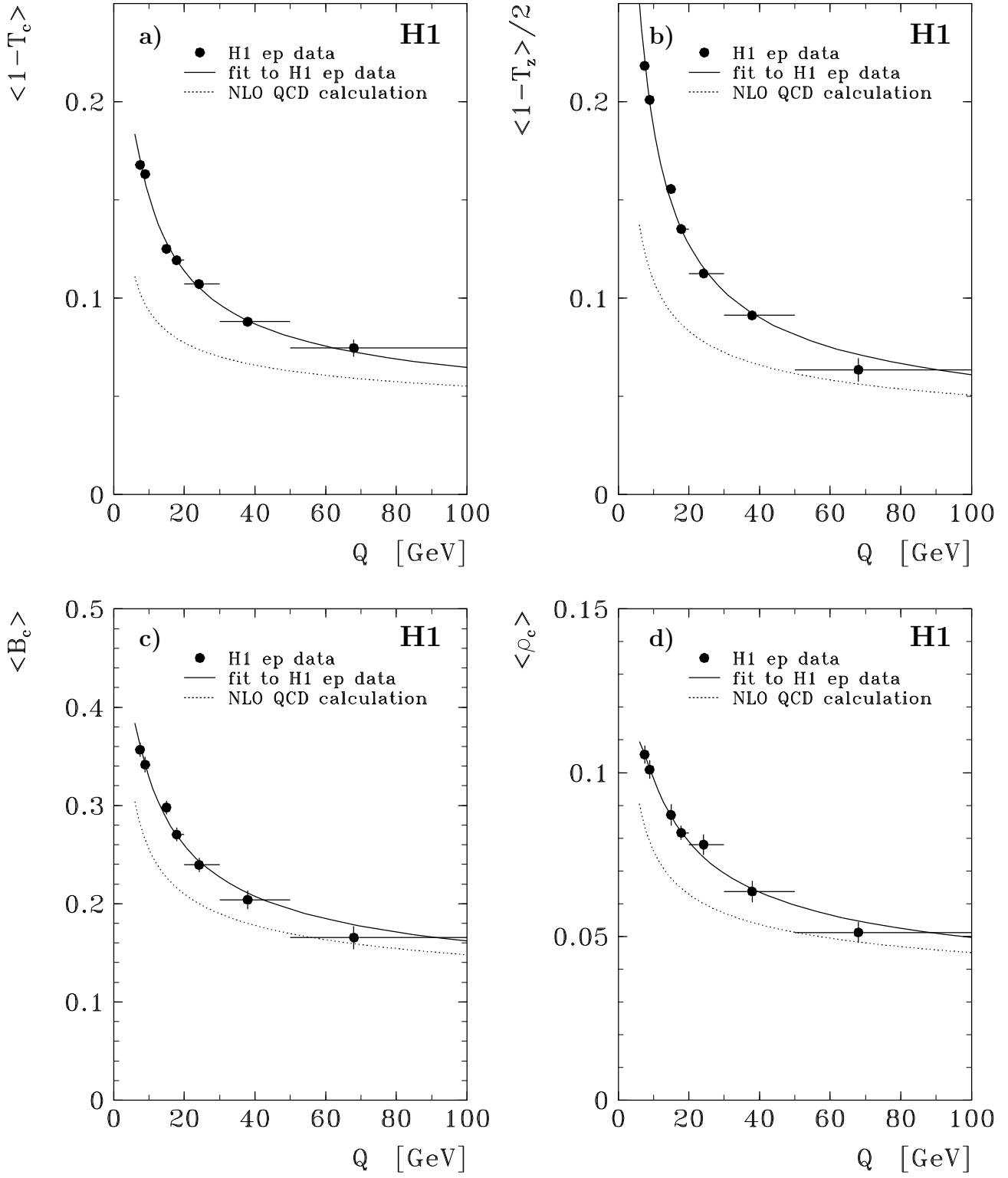


Figure 4: Mean event shape variables as a function of  $Q$  for **a)**  $\langle 1 - T_c \rangle$ , **b)**  $\langle 1 - T_z \rangle / 2$ , **c)**  $\langle B_c \rangle$ , and **d)**  $\langle \rho_c \rangle$ . H1 DIS  $ep$  data ( $\bullet$ , errors include statistics and systematics) are compared with QCD fits ( $—$ ) and second order QCD calculations ( $\cdots$ )